



Observations and Analyses of an Intense Waves-in-Ice Event In the Sea of Okhotsk

John R. Marko

*ASL Environmental Sciences Inc.
Sidney, B.C., Canada
V8L 5Y3*

Abstract

Ice draft, ice velocity, ice concentration and current profile data gathered at an array of 8 continental shelf monitoring sites east of Sakhalin Island were analyzed in conjunction with regional meteorological data to document and explain intense wave occurrences several hundred km inside the Sea of Okhotsk ice pack. The studied event was associated with the March 19-21, 1998 passage of an intense cyclone which produced waves with amplitudes in excess of 1 m at the most offshore monitoring location. The relatively monochromatic character of the waves allowed extraction of wave intensity time series from ice draft time series data. Spatial and temporal variations in these data were used to establish directions and speeds of wave energy propagation for comparisons with an earlier interpretation (Liu and Mollo-Christensen, 1988) of an Antarctic intense waves-in-ice event. It was concluded that, although both events are compatible with a two stage process in which initially slowly advancing wave activity increases subsequent ice cover wave transmissivity, the first stage of the Sea of Okhotsk event was not explicable in terms of the static stress-induced changes in the waves-in-ice dispersion relationship proposed by Liu and Mollo-Christensen. An alternative explanation is offered which eschews the linkage between wave group velocities and the observed slow rates of wave energy propagation and attributes the subsequent transition to more normal wave propagation behaviour to ice pack divergence.

1. Introduction

Large amplitude waves in thick interior pack ice are of considerable relevance both to development and testing of realistic dynamical models of marginal ice zones (Meylan et al., 1997) and, as well, for the safe design and planning of resource extraction and navigation activities in such areas. A prior report of an occurrence of such waves by Liu and Mollo-Christensen (1988) (henceforth to be denoted as LMC) was based upon observations made over a period of many hours during the 1986 Antarctic cruise of the R/V *Polarstern*. In that instance, wave periods and amplitudes of approximately 18 s and 1m, respectively, were estimated to have occurred in 9-10/10 concentrations of highly deformed ice, 0.8 m in mean thickness, located, roughly, 560 km from the closest open water. Anomalously low spatial wavelengths initially characteristic of the event were observed to lengthen with progressive breakup and deformation, eventually approaching

values normally associated with waves of the observed frequency in a deep, ice-free, ocean or in a floating uniform ice cover of moderate thickness.

These observations were interpreted by LMC in terms of the dynamics of an elastic thin plate ice cover. Although the applicability of such an approach to real deformed pack ice was subsequently seriously questioned (Squire, 1995; Rufenach and Liu, 1995), its use apparently yielded explanations of the initial anomalously short observed wavelengths and their subsequent lengthening in terms of phase and group velocities derived from a stress-modified flexural gravity wave dispersion relationship. This treatment required the assumed presence of a static compressive stress component in the direction of wave propagation. The magnitude of this component, as estimated from the initially observed, anomalously short, wavelengths, was shown to reduce the wave group velocity to a near-zero value. High local concentrations of wave energy inferred from the latter result were then assumed to be responsible for subsequent ice breakup and relaxation toward “normal” propagation conditions. As required, the critical stress value was slightly lower than estimates of corresponding buckling and compressive load failure stresses.

The present paper presents and analyzes data recorded during a nominally similar waves-in-ice event which occurred in the Sea of Okhotsk in March, 1998. This event was just one, particularly prominent, example of large amplitude waves which have been detected during recent annual monitoring programs carried out in the same region. In this case, ice and oceanographic data were gathered throughout the event over a wide area with an array of moored sub-surface upward-looking sonar (ULS) instrumentation. Earlier applications of ULS techniques to wave studies both in the absence (De Leonibus, 1963; Macovsky and Mechlin, 1963) and presence (Wadhams, 1978) of sea ice have employed submarines as data-gathering platforms. The data acquired in the present study greatly expanded the spatial and temporal scope of available event information beyond the effectively single-point surface observations considered by LMC. It is our purpose to use these data for detailed documentation of extreme waves-in-ice behaviour and to examine the utility of the LMC theory and an alternative approach for its interpretation.

2. Methodology and Environmental Conditions Accompanying 1997-1998 winter Measurements in the Sea of Okhotsk

2.1 Sub-Surface Measurement Program

The 1997-1998 JIP (Joint Industry Program) Environmental Studies in the Sea of Okhotsk (sponsored by Exxon and Sakhalin Energy) provided measurements of ice-draft, ice-velocity, current profiles and ancillary data on the continental shelf east of Sakhalin Island (Figure 1) at 8 regional sites with the following water depths: Levenshterna, 74 m; PA3, 70 m; PA2, 41 m; PA1, 31 m; AD2, 40.5 m; AD1, 36 m; Chayvo, 26.5 m and Lunskeye, 51 m.

Separate moorings (Figure 2) at each site contained:

- a) an ASL Environmental Sciences IPS-4 Ice Profiling Sonar which sampled ice undersurface ranges @ 1 Hz with a narrow 2°, 400 kHz acoustic beam; and
- b) either: 1) an RDI Workhorse 300Khz ADCP (Acoustic Doppler Current Profiler) with “bottom-tracking” capability which allowed direct measurement of ice drift velocities or; 2), at sites AD1 and PA2, a WHISL (Woods Hole Instrument Systems model SP2000) electromagnetic current meter.

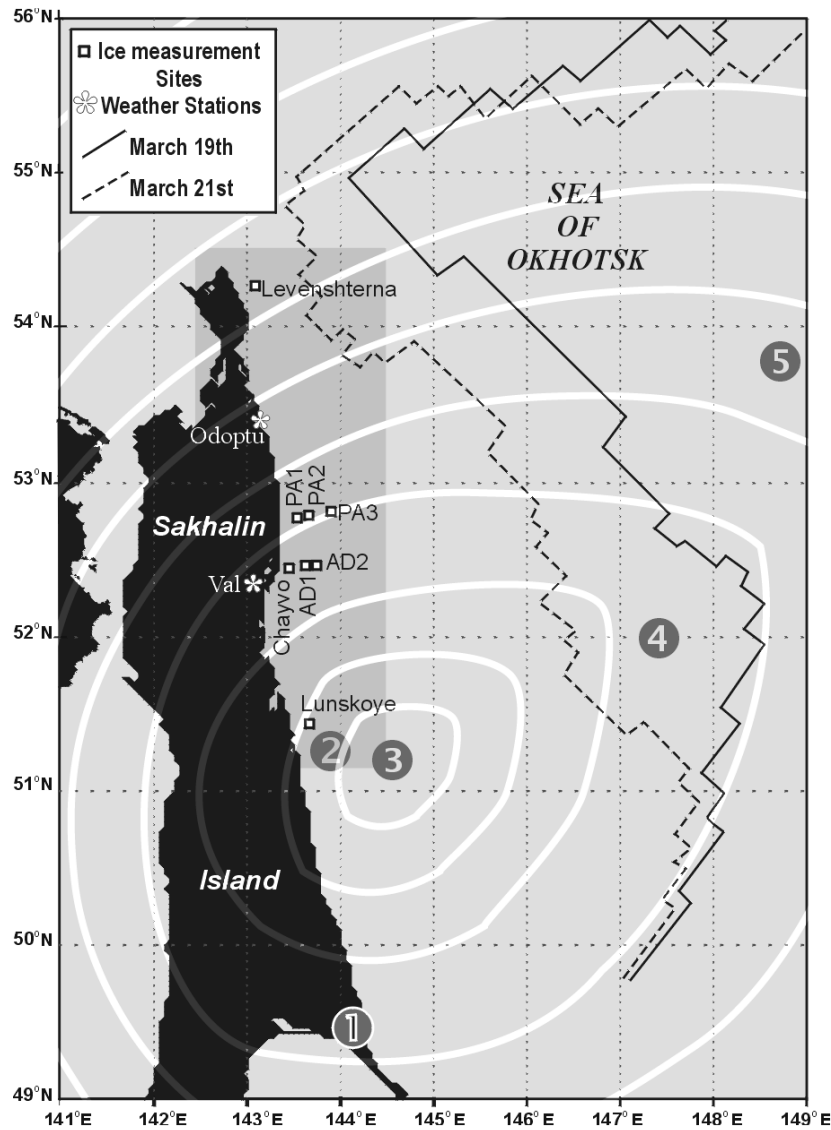


Figure 1. JIP ice monitoring and meteorological sites adjacent to Sakhalin Island in the Sea of Okhotsk. The Figure includes the March 19 and March 21 5/10 ice concentration boundaries and the positions of pressure minima of a traversing cyclone at successively numbered 6-hour intervals between: 1) 0600, March 20, 1998 and; 5) 0600, March 21, 1998. These positions and the superimposed curvilinear lines corresponding to the 1800, March 20 surface pressure contours (at 5 mb intervals from a 965 mb central contour centred at position 3)) were derived from Japan Meteorological Agency Surface Analysis charts.

The separations between moorings at a given monitoring site were short enough (less than 100 m) to assure collection of data representative of a common location. Ranges to the ice undersurface were converted into corresponding draft values using hydrostatic pressures recorded on-board each IPS-4 instrument together with regional surface air pressure data and sound speed estimates updated by occasional measurements of ranges to patches of open water/thin ice (Birch et al., 2000). On-board water temperature and instrument tilt data, as well as CTD profiles obtained during instrument deployments, were also utilized in the conversion process. The resulting draft time series were also translated into draft versus distance representations of ice undersurface topography using ice velocities derived from ADCP or WHISL data sets. ADCP instruments provided data at 10 minute intervals corresponding to 3 minute average current velocities for bins 2 m in depth and ice velocities as averaged over 30 second measurement periods. At the two WHISL-equipped sites, current data were acquired only at a single depth a few meters above the sea floor and yielded outputs of hourly averaged current vectors. Ice velocities at such sites were estimated from the measured current values and contemporary regional wind data using regressions established from data gathered at the closest ADCP-equipped site. Given the superposition of typical 20 cm/s residual ice drift velocities and the large diurnal tidal currents typical of the study area, ice draft data were routinely obtained, with accuracies better than 20 cm, at 50 cm intervals along the ice undersurfaces traversing each site.

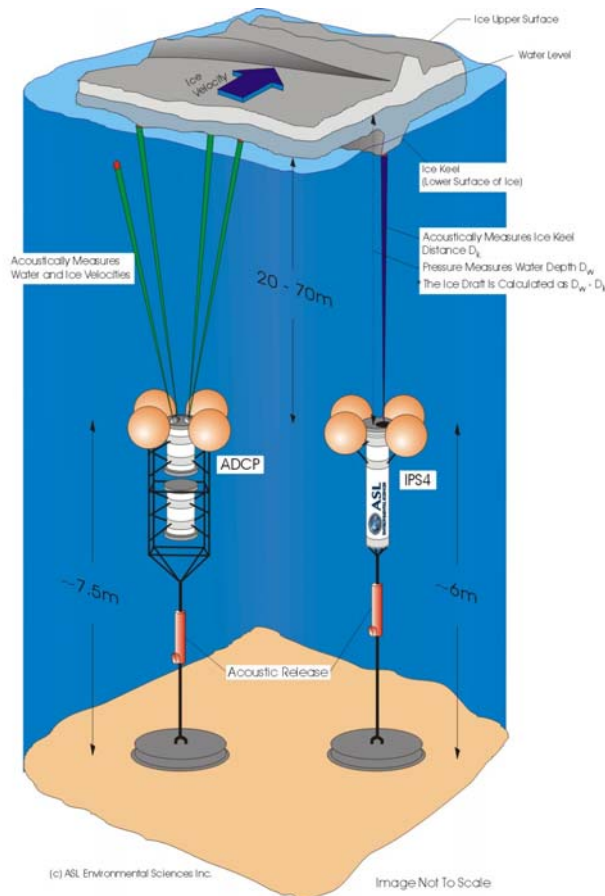


Figure 2. Typical deployment configuration for adjacent IPS-4 and ADCP instruments.
2.2 Meteorological and Ice Conditions

Intense waves-in-ice activity coincided with the N-NE-directed March 19-21 passage of a cyclone over Sakhalin Island and through the Sea of Okhotsk. Positions of the cyclone's pressure minimum, taken from Japan Meteorological Agency Surface Analysis charts, are denoted in Figure 1 at 6-hour intervals for the shorter period, 0600, March 20 through 0600, March 21 (all times are referenced to Universal Coordinated Time (UTC)) associated with the build-up and peak intensity phases of the waves-in-ice event. To illustrate the spatial scale of the atmospheric forcing, this Figure also includes pressure contours corresponding to 1800, March 20 when the central pressure minimum reached an overall event minimum value of 964 mb. The plotted positions show that the depression moved from about 200 km south of the study area to locations, respectively, roughly 20 km SE and, then, 50 km E-SE of the southernmost, Lunskeye, monitoring site prior to E-NE and NE movements over the outer reaches of the pack ice after 1800, March 20. Accompanying changes in surface pressure, wind direction and wind speed are evident in the Val (52° 20' N, 143° 05' E) coastal station data of Figure 3.

Although cloud coverage precluded useful satellite observations during the waves-in-ice event, a March 19 NOAA AVHRR image showed the extreme northern and southern sites under heavy, 9/10-10/10, ice as well as slightly lower ice concentrations at the central sites, primarily in the form of what appeared to be, within the 1 km resolution of the imagery, individual floes with linear dimensions ranging upward to 10 or 15 km. The latter, larger, floes in the image had exhibited little detectable change in size and shape over the previous few days but it is possible that such features were relatively weakly bonded agglomerates of smaller floes. The westernmost central sites, PA1 and Chayvo, were under ice at the eastern edge of a large coastal polynya. The effects of subsequent dramatic changes in the regional pack over the next 2 days were evident in mappings of ice concentrations derived on March 19 and 21 from 25 km spatial resolution SSM/I passive microwave data acquired by a Defence Meteorological Satellite Program (DMSP) satellite. As indicated by the contours of the 5/10 (50%) concentration boundary plotted in Figure 1, these data were consistent with a massive, approximately 80 km, westward shift of this boundary in areas east of the central sites over the intervening period. Nevertheless, even after this shift, presumably driven by the March 20 easterly wind forcing (Figure 3), on March 21 ice at concentrations lower than 5/10 came no closer than 155 km to the nearest central monitoring site (PA3). With the 1.6/10 (16 %) ice concentration boundary (Figure 4) lying a further 185 km offshore, the PA3 site was more than 300 km from open water in the eastern Sea of Okhotsk throughout the waves-in-ice event. U.S. National Ice Center chart data suggested ice was present in the 30-70 cm and 70-120 cm thickness categories prior to March 20. IPS-4 draft and concentration data showed high concentrations of considerably thicker ice to be present at all sites during the event. Specifically, at the 6 central sites hourly-averaged drafts for the period 1600, March 20 to 0000, March 22, (Figure 5) increased in the westerly and northerly directions and only occasionally failed to exceed 1 m. Drafts in excess of 2m were common at PA1, PA2 and Chayvo. Still larger average draft values were encountered, at times, at the Levenshterna site.

At all sites, concentrations deduced from the IPS-4 records rarely descended below 9/10 (90%) and then only at the most offshore and southern central sites, AD1 and AD2 and at Lunskoye.

The absence of acceptable quality satellite imagery during the event precluded detailed documentation of changes in floe sizes during the studied event period. Nevertheless, AVHRR imagery from the relatively slowly moving ice pack in the March 22-25 period was suggestive of an overall reduction in floe size relative to the March 19 pre-event period.

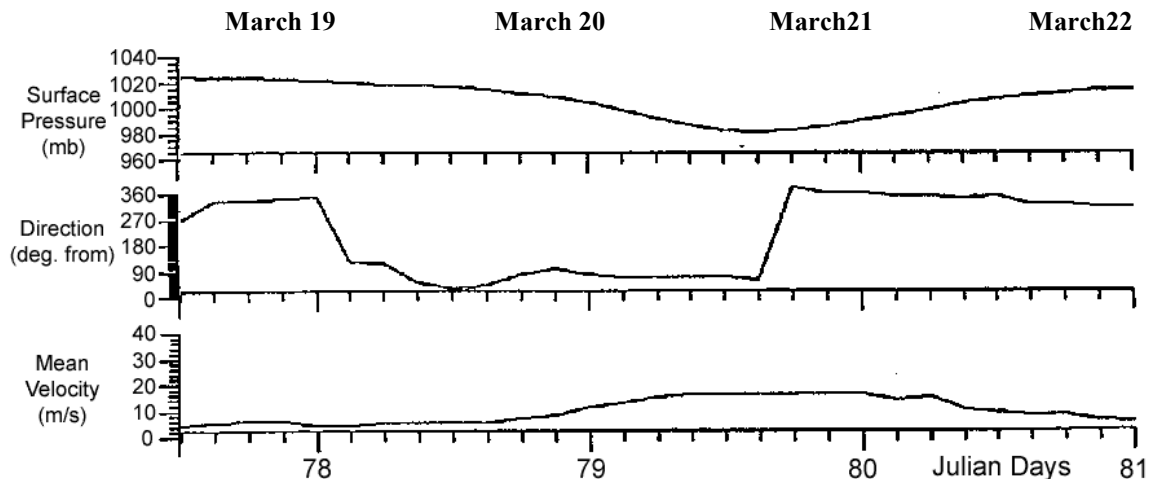


Figure 3. Meteorological data recorded at Val

Progressive displacement plots for ice at the six ADCP-equipped monitoring sites for the period 1200, March 19 to 0000, March 22 (Figure 6) showed the inferred rapid westward ice movements at the central sites began at, roughly, 0000, March 20 (Julian Day 79.0) and persisted until about 1800, March 20. These movements corresponded to an overall average westward speed component of about 40 cm/s (0.8 kt). The net displacements at the 6 ADCP-monitored sites for the 0000-1800, March 20 period of westward drift (Table 1) show the greatly reduced magnitudes of this drift at the peripheral Levenshterna and Lunskoye sites. As well, it should be noted that, except near Chayvo where the initial width of the polynya was exceptionally large, net westerly drift decreased in the shoreward direction. This observation and the fact that displacements at all central sites were several times smaller than the contemporary 80 km mean shift in the position of the 5/10 concentration boundary (Figure 1) were consistent with westward increasing resistance to ice drift arising from the closing of the coastal polynya and the observed shoreward thickening of the ice pack. It is also significant that southward ice drift at the central sites only reappeared after, roughly, 1500, March 20, coincident with the easterly to northerly wind rotation at Val and the eastward shift of the cyclone away from the Sakhalin coastline.



Figure 4. The 64%, 50%, 29% and 16% ice concentration contours as derived from March 21, 1998 SSM/I imagery.

3. Waves-in-Ice and Current Data

With the outermost, PA3, site at least 150 km west of the 5/10 concentration boundary and 9-10/10 concentrations of 1.35 m to 2.5 m thick ice present in the central study area, initial evidence of large amplitude, periodic wave-like components in the time series draft records was viewed with some skepticism. Although, as noted above, similar events have since been detected in subsequent annual Sea of Okhotsk data sets, additional caution was suggested by the initially perceived absence of similar activity at the northern Levenshterna site. The latter site was only 35 km inshore of the 5/10 ice boundary and, in view of the large spatial scale of the cyclonic depression (Figure 1) might have been expected to have been exposed to local wave conditions at least as severe as those attained at the central sites. Nevertheless, PA3 time series results (Figure 7) showed unambiguous periodic and negative-going draft variations consistent with wave-driven vertical oscillations of the ice undersurface. Moreover, these oscillations had appropriate counterparts in the IPS-4 hydrostatic pressure data records.

Spectral analyses (Figure 8) of data recorded at times roughly coincident with peak wave intensities along the northern line of central sites, PA3, PA2 and PA1, showed the wave activity to be narrowband and centred at approximately 0.07 Hz (14 second wave period). The displayed spectra were derived from draft time series after initial processing with a high pass filter (characterized by 30 dB stop band rejection and a cutoff frequency of 0.025 Hz) to diminish the contribution of ice topography to overall range variance. This step reduced “leakage” into the wave related peaks of interest from the strong topographically-related spectral components which increased monotonically in intensity with decreasing frequency down to zero frequency. An unfortunate side effect of the high pass filtering was the introduction of an artificial “peak” into each of the displayed spectra just above the cutoff frequency. The larger amounts of ice deformation characteristic of the more shoreward PA2 and PA1 sites relative to PA3 were responsible for the larger artificial peaks associated with these sites. Nevertheless, the wave-related

peak was readily distinguishable from the truncated low frequency topographic contributions for all central sites. The spectral results (Figure 8) showed both narrowing of the wave spectrum and progressive attenuation of wave energy with increasing distance from the presumed eastern wave source areas. The character of the spectral narrowing, i.e. shoreward reductions in the higher frequency components of the wave-related peak, was fully consistent with the expected behaviour of the ice medium as a low-pass wave filter.

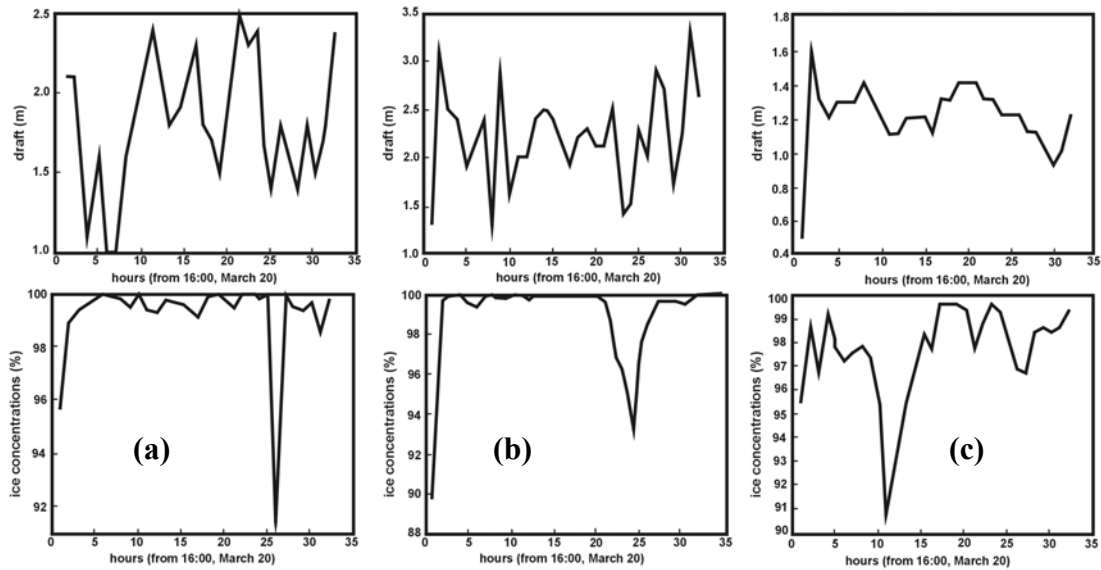


Figure 5a-c. Hourly averaged ice drafts and concentrations at hourly intervals beginning at 16:00, March 20 as estimated from IPS-4 data recorded at : a) PA1, b) PA2 and; c) PA3.

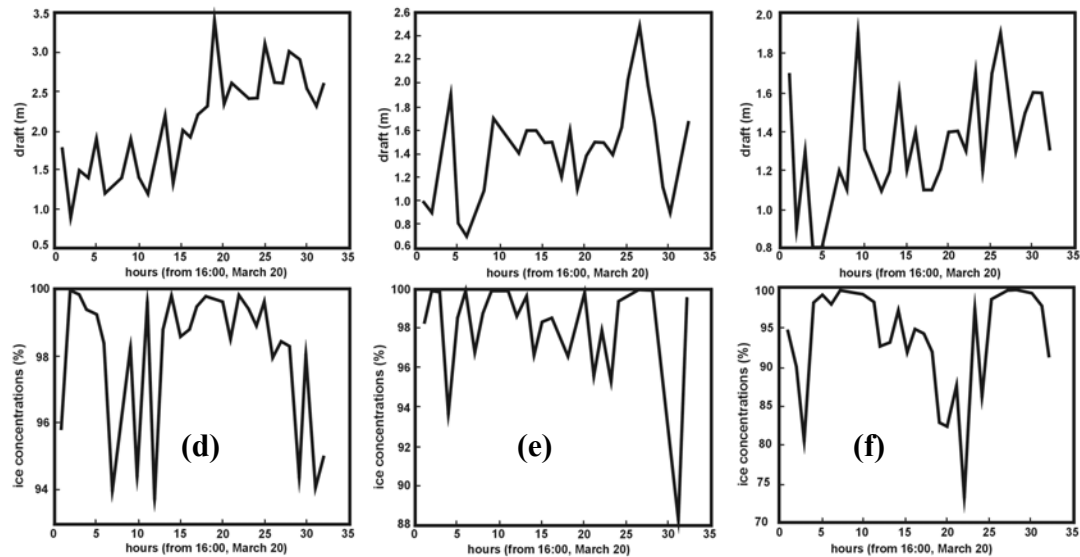


Figure 5d-f. Hourly averaged ice drafts and concentrations at hourly intervals beginning at 16:00, March 20 as estimated from IPS-4 data recorded at : d) Chayvo, e) AD1 and; f) AD2.

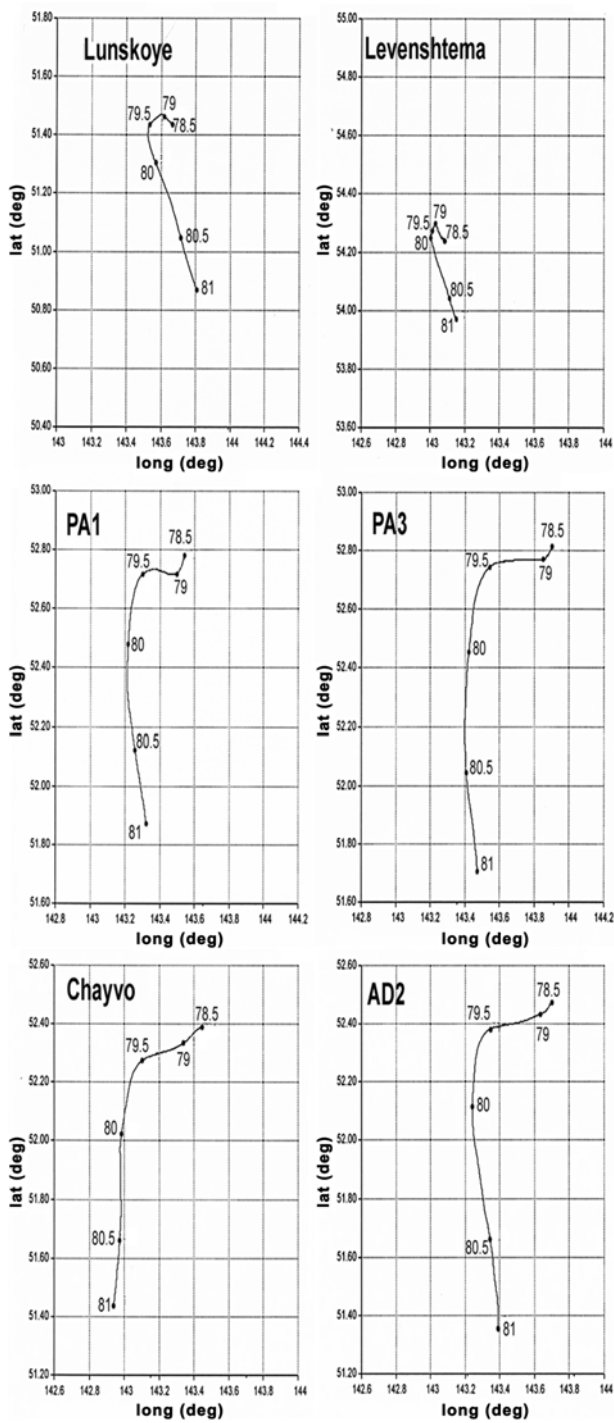


Figure 6. Ice drift at the 6 indicated sites in the period between 1200, March 19 (Julian Day 78.5) and 0000, March 21 (Julian Day 81.0).

Site	Net Westward Displacement in km over 0000-1800, March 20 (Julian Day 79.0-79.75)
Levenshterna	2
PA-3	27
PA-1	17
AD-2	26
Chayvo	29
Lunskoye	5

Table 1. Westward ice displacements at ADCP ice-tracking sites

The narrow spectral range of the oscillatory behaviour facilitated separation of wave- and ice-topography-related components of the draft time series data. Temporal and spatial variations in the wave-related signal components were quantified through applications of, first, a common digital band-pass filter with 40 dB rejection and 0.066 Hz and 0.078 Hz half power points to all draft time series, followed by squaring of individual data values and low pass filtering to suppress variability on time scales longer than, roughly, 2 hours. Detailed intensity (defined as the low-pass filtered square of band-passed draft amplitude) versus time results are plotted in Figure 9 for all sites for the period 0000, March 19 to 1600, March 23. This Figure also includes representations of near-surface total (tidal + residual) current vectors for the shorter 0600, March 20 through 0000, March 22 time interval associated with all but the terminal stages of the waves-in-ice event. The currents plotted for each of six ADCP-equipped sites are representative of values at 6-8 m depths at 10-minute intervals. WHISL results for the other two sites are provided as hourly-averaged current vectors. The full body of profile results showed the water flow to be essentially barotropic during the event, allowing the near-bottom currents plotted for the latter sites to be representative of current variability in the local upper water column.

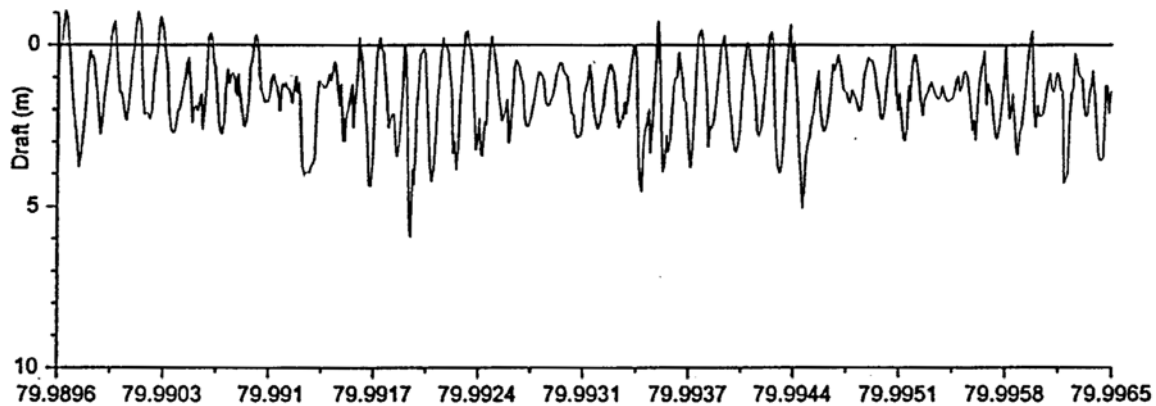


Figure 7. Ice draft time series for the site PA3 during a 10-minute period centred on Julian Day 79.9931 (2350, March 20, 1998).

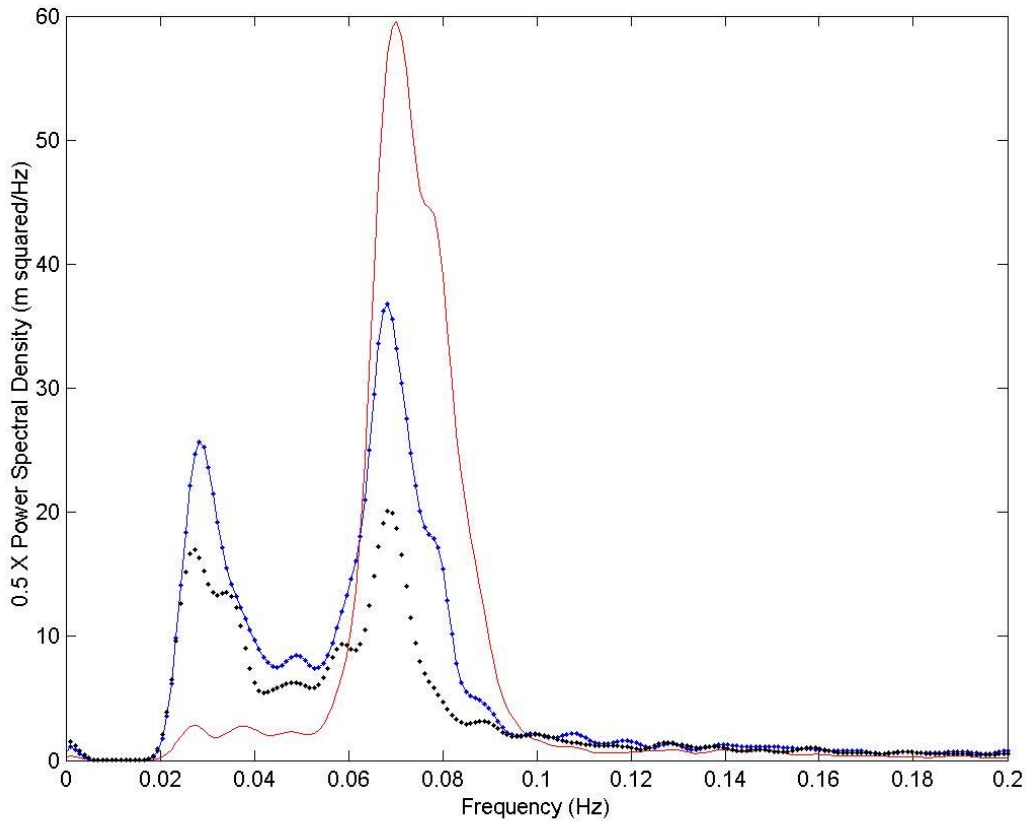


Figure 8. Temporal spectra for periods encompassing peak activity at: PA3 (solid line, 0144- 0532, March 21); PA2 (connected dots, 0301-0712, March 21) and PA1 (unconnected dots, 0238-0712, March 21). All draft times were subjected to high pass filtering with 30 dB rejection and an upper cutoff at 0.025 Hz to eliminate power “leakage” from high intensity low frequency spectral components associated with the ice undersurface topography. This truncation gives rise to the artificial peaking of the spectrum adjacent to the cutoff frequency.

The wave intensity data show that the first signs of a waves-in-ice event appeared at the Lunskeye and PA3 sites at about 1800, March 20. Alternatively, the latest first appearance of wave activity at any site occurred at Levenshterna, although the wave signals detected at this location and at the other peripheral, Lunskeye, site were only modestly above background levels. As inferred above for the PA sites (Figure 8), intensities were progressively decreased in magnitude and delayed in arrival in the shoreward direction. No universal “shape” or time dependence was apparent among the individual site wave intensities. Differences in this respect were particularly evident between inshore (PA1 and Chayvo) and offshore (PA3, PA2, AD2, AD1) sites. Specifically, inshore sites showed longer durations of wave activity and intensity fluctuations of characteristically larger amplitudes and lower temporal frequencies (≈ 7 cycles/day) relative to offshore sites.

The current data in Figure 9 show enhancements of the prevailing strong southward flows were initiated shortly before 1800, March 20 at the more southern and inshore sites (Lunskeye, Chayvo and PA1), with maximal near-surface flows increasing in a north to

south direction and peaking at speeds between 60 and 100 cm/s. The increase in the southward current component was, roughly, coincident with the above-noted switch to northerly winds and the appearance of strong southerly ice drift components. As in the ice drift results, current changes were greatly diminished and delayed by about 16 hours at the northern, Levenshterna, site.

Reviews of the combined data sets suggest that an enhanced local southward current presence was a necessary but not sufficient condition for detectable local wave activity. Likewise, wave activity at times within 1 or 2 hours of local southward current increases was characteristic of sites which were either closest to the 5/10 ice concentration boundary (Levenshterna and PA3) or lay inshore of ice largely excluded from earlier intense westward ice drift (Lunskoye). As well, it is notable that peripheral site (Levenshterna and Lunskoye) wave intensities exhibited no obvious dependences upon southward current strength in contrast to the central sites where intensities peaked well after large increases in southward flow and within a few hours of maximal current speeds.

4. Data Analyses and Interpretation

4.1 Interpretation of Wave Propagation Results

Efforts to understand the origins of the observed waves-in-ice event were complicated by the noted site-to-site differences in the temporal variability of wave intensity¹. These differences precluded use of simple cross-correlations for estimating wave propagation speeds and directions. Instead, propagation was quantified by assuming one to one correspondences among first signal arrivals at all individual sites (i.e. the relative delay between first arrivals at any two sites was taken as a measure of the velocity of wave energy propagation over the intervening distance). These first arrival times were established ignoring time series data corresponding to intensities smaller than roughly 0.015 m² which preceded the sharp initial rises in intensity observed at all central sites (Figure 9). This restriction ruled out detailed timing estimates for the marginal intensity signals detected at the two peripheral sites. At the central sites, however, arrival times, defined by intersections of the time axis with straight-line projections of the initial sharp intensity rises, allowed calculation of effective wave signal delays for specific paths connecting pairs of monitoring sites.

Actual computations of propagation parameters were carried out separately for three different groups of 3 sites as listed in Table 2. Each group is representative of an identifiable portion of the central study region (Figure 10). Timing and amplitude

¹ Inhomogenities in the seaward ice pack were a likely major source of the noted differences in the forms of individual intensity vs. time data plots (Figure 9). Attempts to establish consistent cross-correlations between wave packets as observed at even the closest adjacent sites, AD1 and AD2, (separated by about 3 km in the anticipated east-west wave arrival direction) were not successful. This result was suggestive of the presence of large variations in the amplitude of the oscillations as a function of position along a given "wavefront". Similar variations were apparent in the signatures of waves propagating through similarly thick ice on an April 25, 1997 Radarsat image of the study area (Marko, 1998).

differences were computed for the 2 separate, non-parallel paths linking different sites in each group to its common “vertex” site. These differences allowed unambiguous estimation of parameters describing the propagation of parallel wavefronts through the three sites of each group. The group containing paths PA3-PA2 and PA3-AD1 provided data representative of waves in the outer portion of the monitoring array (36 m to 70 m water depths). The other two groups, comprised of the PA2, PA1 and Chayvo sites and the AD1, PA1 and Chayvo sites, are similarly representative of the northern and southern ends, respectively, of the more inshore (26 - 40 m deep) monitoring regime. The resulting propagation parameters, listed in Table 2 for all three groups, include the speed, s , and direction, θ , of wave propagation as defined in terms of positive clockwise rotations from a due-westward reference direction. Separate values of attenuation coefficients, α , are also listed corresponding to wave amplitudes, A , satisfying:

$$A(x)/A(x=0) = e^{-\alpha x} \quad (1)$$

for displacements, x , in the direction of wave propagation. These quantities were calculated from the ratios of amplitudes associated with peak wave intensities at the two sites terminating each of the two paths in a given group. RMS values of these peak amplitudes, A_{peak} , ranged between 0.59 m (Chayvo) and 1.08 m (PA3). The latter value, observed in ice of approximately 1.35 m average thickness, is equivalent to a 4.32 m significant peak to peak wave height. Actual computation of α values from peak amplitude ratios required division by the cosines of the angle between the path and the inferred propagation direction (θ). The, roughly, 0.5 hour uncertainties in estimated signal arrival times limited the accuracies of the obtained wave directionalities and speeds to approximately +/- 3° to 4° and +/- 10 %, respectively.

Group Vertex	Other Member Sites	s (m/s)	θ (°)	α (10^{-5} m^{-1}) by member pair
PA3	PA2, AD1	1.85	-7.4	1.30 (PA3-PA2), 1.49 (PA3-AD1)
PA2	PA1, Chayvo	0.72	+4.0	5.36 (PA2-PA1), 5.22 (PA2-Chayvo)
AD-1	PA1, Chayvo	1.17	+1.6	1.52 (AD1-Chayvo), 3.08 (AD1-PA1)

Table 2. Propagation and amplitude attenuation parameters for waves-in-ice as derived from non-parallel measurement paths connected to the indicated group vertex.

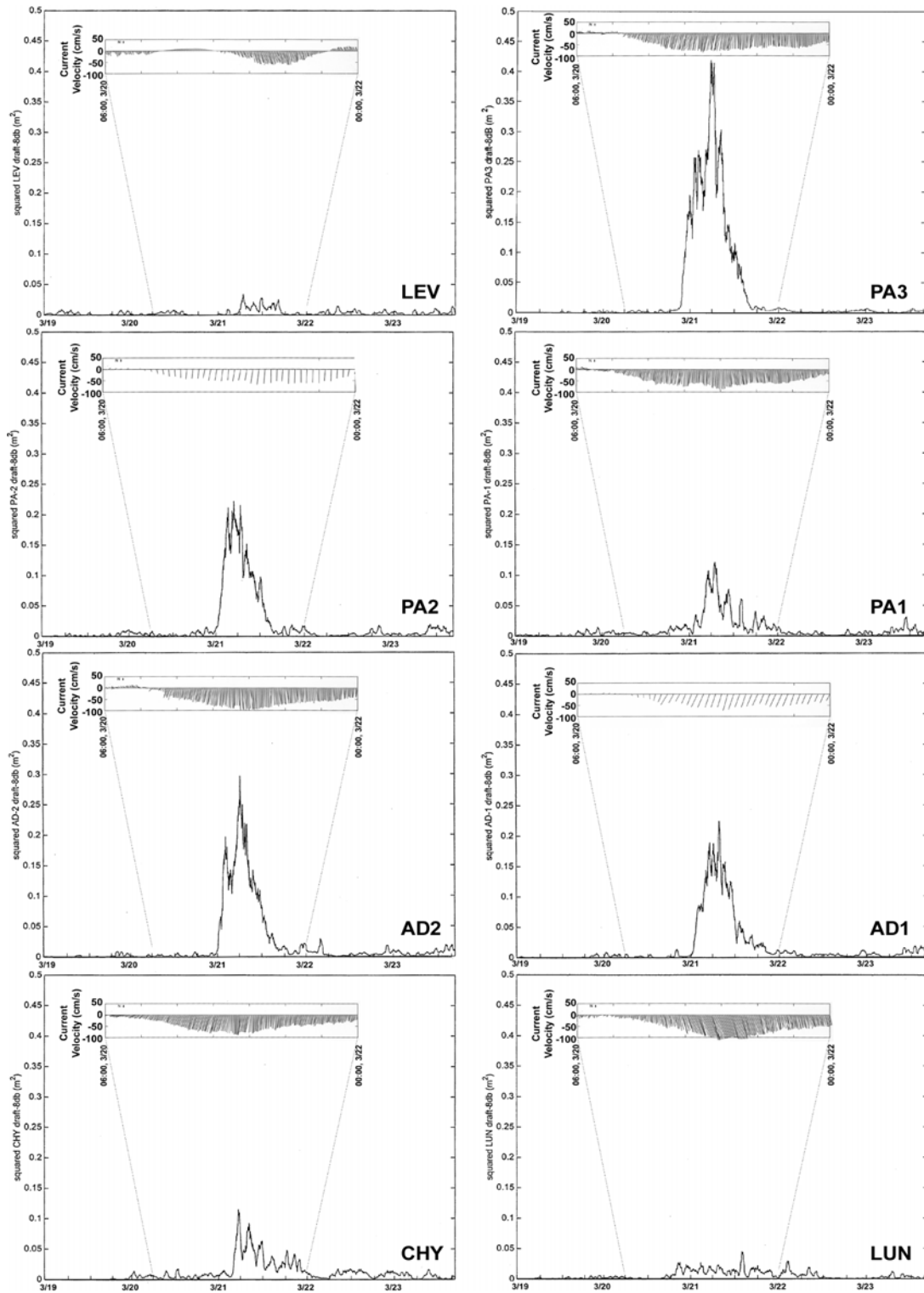


Figure 9. Filtered wave intensity-8dB plotted as a function of time in the period; 0000, March 19 – 1600, March 23 for each JIP site. Stick plot representations of total (residual + tidal) currents are also included in each case as indicated for the period, 0600, March 20 through 0000, March 22.

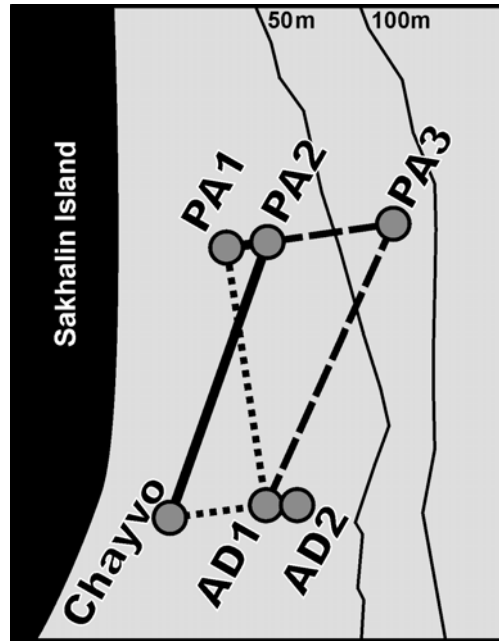


Figure 10. Groupings of central sites for propagation calculations. The solid, dotted and dashed line connect pairs of sites associated with, respectively, the PA2, AD1 and PA3 vertices. Water depths associated with the each vertex group may be inferred from the included bathymetric contours.

Two of the three parameters listed in Table 2, namely θ and α , the wave directionality and attenuation rate, respectively, are reasonably consistent with expectations. Thus, the values of θ confirm the anticipated almost due westerly wave propagation directionality and offer slight evidence for a small but consistent rightward (northward) turning in the more western and northern AD1 and PA3 vertex areas associated with shallower waters and thicker ice. The attenuation coefficients for the outermost, PA3, vertex region are comparable to values reported (Squire and Moore, 1980; Wadhams et al., 1988) for a stable (i.e. not undergoing break-up) Bering Sea ice cover. In that instance, the assumed distribution of ice thicknesses was indicative of somewhat lighter conditions (0.8 m vs 1.35 m mean ice thicknesses and 7/10 vs 10/10 concentrations) relative to our measurement locale. Applying the Wadhams et al. (1988) theoretical ice thickness- and concentration-dependences to effect adjustments between the two data sets suggests the intrinsic attenuation rates of the present study fell below comparable Bering Sea values by, roughly, a factor of three. This discrepancy is not greatly outside of the combined measurement uncertainties in the two bodies of data and could be indicative of the limitations of our estimation technique which focused on peak intensities and applied a fixed bandpass filter to signal inputs with position-dependent spectral composition (Figure 8). As well, a simple assumption of the presence of larger floe diameters (80-90 m versus 20-30 m) in the Sea of Okhotsk study could also account for the inferred differences, given the theoretical floe size dependences derived by Wadhams et al. (1988). Although, as noted above, detailed data of floe size distributions during the wave event were not available, IPS4 data from the post-event period, presented in the following sub-section, are not inconsistent with this assumption. The larger values of α deduced for the PA1 and AD1 vertex areas are (ignoring the discrepancy between the 2 alternative estimates for the AD1 vertex) also within a factor of 2 to 3 of comparable Wadhams et al.

(1986) estimates made for several East Greenland Sea areas occupied by ice of various concentrations with thicknesses on the order of 3 m.

On the other hand, values of the third parameter listed in Table 2, the speed, s , of wave energy propagation, are anomalously low relative to expectations for either ice-free or ice-covered oceans. Specific comparisons were made with theoretical group speeds derived using a dispersion relationship (Fox and Squire, 1990) appropriate to flexural gravity waves propagating in a uniform continuous ice sheet modelled as a thin elastic plate. Employing mean thickness values derived from Figure 5, our calculations yielded theoretically expected group speeds of 12.07 m/s, 11.83 m/s and 11.64 m/s at the approximately 70 m, 40 m and 30 m water depths associated with the progressively more shoreward PA3, PA2 and PA1 sites. The small differences in these group speeds suggest that the effective attenuation rates between the PA3 and PA1 sites could have been underestimated by, at most, two per cent as a consequence of wave energy conservation-induced wave steepening (i.e. in the absence of dissipation, the product of wave energy per square meter and the group speed is conserved). Further, since the group velocity associated with the ice-free- or thin ice-covered-deep ocean, 10.9 m/s, falls below the group velocities expected at the ice-covered monitoring sites, wave steepening can be excluded as a contributor to propagation of offshore wave energy into our study area.

4.2 Development of a Basic Interpretative Model

The character of these results readily facilitates interpretation in terms of a two stage process in which an incident, slowly advancing, wave disturbance breaks up and alters the properties of an ice regime which had previously highly attenuated incident gravity waves. The consequent changes lower the effective attenuation coefficients to the values listed in Table 2 on the basis of comparisons of peak amplitudes at adjacent sites. These coefficients are associated with propagation in the second stage of the event and are roughly compatible with earlier marginal ice zone measurements and with expectations from multiple wave scattering theories (Wadhams et al., 1988). The LMC interpretation of the 1986 Antarctic waves-in-ice event, outlined in Section 1, is an example two stage process.

In evaluating the relevance of any two stage approach to the Sea of Okhotsk event, it is sensible to begin by examining the compatibility of the second “normal” propagation stage with observational details. The characterization of the pack during this period as a collection of individual floes is consistent with the prevalence of southerly currents and ice velocities during the post-1800, March 20 period of significant observed wave activity. The positive north to south gradient in ice velocities characteristic of this period and the disappearance of the preceding strong westward drift would have facilitated divergence and gradual dispersal of an ice pack which had previously been transformed into a highly compacted and deformed state by intense easterly wind forcing in the direction of the Sakhalin Island coastline. Although these changes have been largely inferred from very limited and low resolution satellite data and from the atmospheric and oceanographic data sets, additional, more direct, measures of corresponding differences in ice cover structure are available from the IPS4 data records. These measures lie within

the distributions of the spatial separations between successive occurrences of open water/thin ice as encountered along the linear draft versus distance profiles (Section 2.1) created by combined use of ice-draft and -velocity data. In all cases, such separations (derived using a draft threshold of 15 cm for open water/thin ice areas) were extracted from 35 to 45 km long ice cover segments as monitored at individual sites during:

- a) the 0.75 to 1 day pre-event periods defined by the interval between the start of the strong easterly wind forcing and early wave arrivals at each site; and
- b) the 1.5 to 2 day periods immediately subsequent to the decay of local wave amplitudes to levels insignificant relative to local ice draft variations.

These data provided quantitative characterizations of local ice covers during, respectively, the postulated ice pack compression and during the subsequent slow drift of a dispersed (but still highly concentrated) ice pack. No equivalent analyses were carried out for data gathered coincident with the intervening wave activity at a given site in order to avoid the complications introduced into identification of open water/thin ice areas by the presence of large wave-driven vertical ice displacements.

Histograms associated with pre- and post-event separations at the three PA sites (Figure 11) show significant increases in the prevalence of smaller open water/thin ice separations (expressed as percentages of the total lengths of the surveyed tracks) introduced by local wave events. In fact, linearly sampled separations of adjacent open water/thin ice occurrences, such as represented by the data in Figure 11, can provide estimates (Rothrock and Thorndike, 1984) of local floe size distributions within the limitations imposed by simplifying assumptions on floe- shape, - anisotropy and -orientation (and, again, assuming absence of detectable open water/thin ice implies ice continuity). Within the simplest, circular floe, assumption, the histogrammed data suggest that the initial wave arrivals in the March, 1998 event encountered an ice cover characterized by a preponderance of floes with diameters exceeding 500 m, reflecting the effectiveness of the identified pre-event compressive wind forcing. Moreover, larger floes continued to be the dominant feature of the ice pack throughout the wave event and in the immediate post-event period. Nevertheless, the results also suggest that in the latter two periods, roughly 50 % of a given wave propagation path at the two most shoreward PA sites (PA1 and PA2) traversed floes with diameters smaller than 500 m. In fact, a reasonable estimate for the mean diameter of these smaller floes would appear to lie somewhere in the vicinity of 150 m and is hence not greatly inconsistent with the 80 to 90 m diameter floe diameters which, as noted in the previous sub-section, would make our estimates of wave attenuation in the PA3 vertex region compatible with earlier results (Squire and Moore, 1980; Wadhams et al., 1988). The higher prevalence of larger separation/floe diameter values at the PA3 site in Figure 11 is believed to be an artefact of the extremely broken nature of the post-event ice at this site. Corresponding quasi-spatial profiles computed for the site in this period most closely resembled a rubble-field, exhibiting closely packed shallow keels with horizontal linear dimensions on the order of 2m or less and with frequent sections where drafts lie just above our 15 cm threshold. Consequently, the effective dimensions of floes relevant to wave propagation may have been considerably smaller than implied by the separations of the detected open water/thin ice areas at this site.

Given this additional confirmation of our basic picture of the wave event circumstances, it remains to examine the proposed assumption of “normal” wave propagation through concentrated dispersing ice floes in the second stage of the event. This effort is carried out in the following two subsections which, respectively, attempt to explain the wave amplitude and timing associated with the transition to second stage propagation at the outermost, PA3, site and to identify a candidate mechanism for the noted differences in wave intensity variability between inshore and offshore monitoring sites. A final subsection considers the more problematic first stage of the proposed model in order to evaluate the compatibility of the observational data with the LMC model and an alternative interpretative approach.

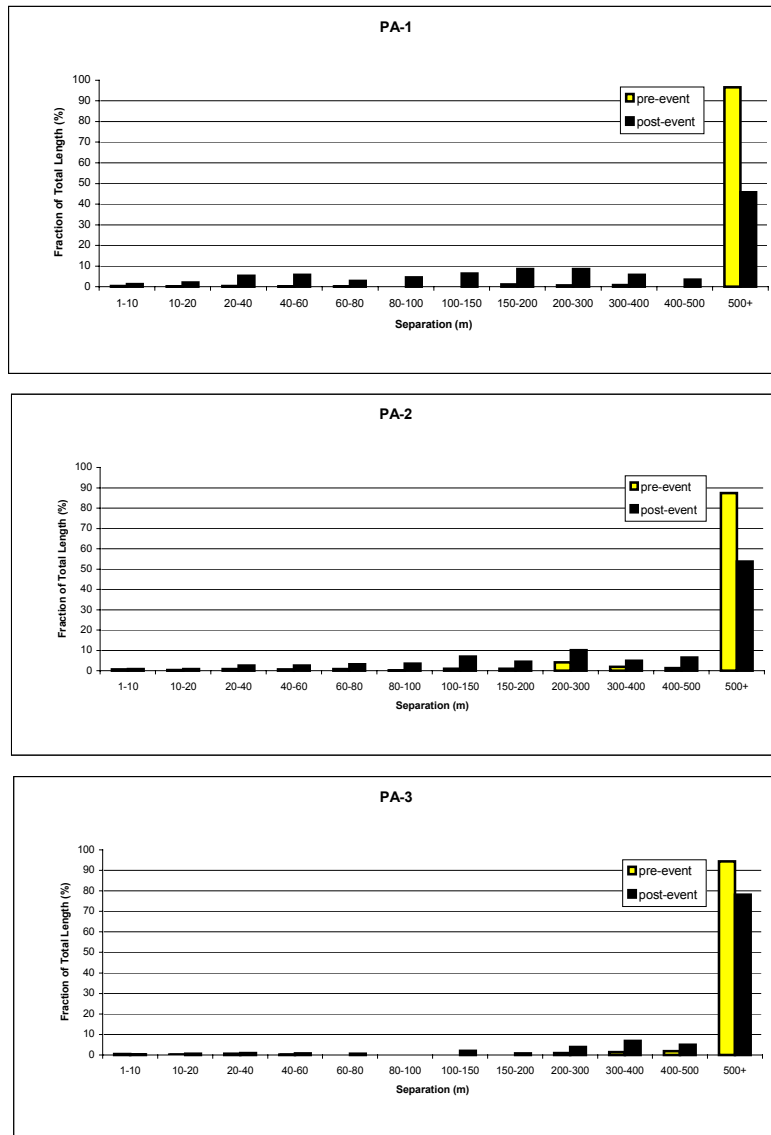


Figure 11. Histograms of percentages of total profile length as a function of separations of consecutive open water/thin ice area occurrences as computed for the pre- and post-event periods at sites PA1, PA 2 and PA3.

4.3 Wave Activity at PA3: Compatibility with Meteorological Data and “Normal” Propagation through Floe Ice.

A minimum requirement for the second stage of the model is that the observed/inferred atmospheric forcing in the offshore wave source areas should have been capable of producing waves at PA3 with amplitudes at least equal to those observed at times shortly after the postulated transition to “normal” wave propagation. Establishing the timing of the latter transition is not straightforward, given the circumstances of a progressively changing, inhomogeneous ice pack accompanied by similarly variable forcing conditions in the wave source areas. A reasonable choice in this regard is to associate the transition with the 0130, March 21 leveling off of the initial intensity rise (Figure 9). This transition step preceded actual peak site wave activity by, roughly, 3.5 hours. The PA3 wave amplitude at this time, equal to approximately 0.8 m, was used to establish minimum sea state requirements for the wave source areas at an appropriate earlier time for comparisons with a wave hindcast. A critical step in this process was the characterization of ice conditions seaward of PA3 as specified in Table 3 on the basis of the March 21 SSM/I ice concentration mapping (Figure 4). Listed parameters include the separations (ΔL_i) between the inshore and offshore edges of 3 different ($i = 1, 2, 3$), successively more eastward, ice zones separating PA3 from the approximate 22% concentration contour. (Ice concentrations beyond (east of) the latter contour were assumed to be low enough to allow open-ocean wave generation capabilities.) The (assumed) north-south oriented inshore edge of Zone 1 includes the PA3 site and is identified with 100% ice coverage. Other listed entries include the lowest (C_{iL}) and median (C_{imed}) concentrations as well as corresponding mean thicknesses (h_i) in each zone. The latter values were estimated conservatively (i.e. tending toward overestimation of outer region thicknesses) assuming a gradual eastward decrease from a thickness, $h_{PA3} = 1.35$ m, deduced from the PA3 hourly-averaged draft results (Figure 5) for times close to the assumed start of stage 2 behaviour.

Zone (i)	C_{iL} (%)	C_{imed} (%)	h_i (m)	ΔL_i (km)
1	64	80	1	40
2	50	57	.75	115
3	22	36	.5	62

Table 3. Characterization of ice offshore of PA-3 on March 20-21 as estimated from the March 21 SSM/I ice mapping.

Attenuation coefficients were estimated for each zone using the above-noted (Wadhams, 1986) linear concentration and thickness dependences in the form:

$$\alpha_i = [C_{imed}/100] (h_i/h_{PA3}) \alpha_{PA3} , \quad (2)$$

with α_{PA3} representing the mean attenuation coefficient ($1.4 \times 10^{-5} \text{ m}^{-1}$) previously estimated for the PA3 vertex region (Table 2). Successive applications of Eqs. (1) and (2) to progressively more offshore zones established that .8 m amplitude waves at PA3 would have required wave amplitudes of 2.2 m, equivalent to a peak to peak significant

waveheight of 8.8 m, at the offshore edge of the easternmost, $i = 3$, ice zone. Further, for such waves to be the sources of the wave intensities observed at PA3 at 0130, March 21, these sea states would have had to be present in the source area T hours previously, where T is the time required for subsequent propagation to PA3. An estimate of $T = 5.5$ hours was obtained based upon our model's assumption of conventional ice-ocean wave propagation, corresponding to an 11.5 m/s group velocity which is midway between values expected for, respectively, 14 s waves at PA3 and in the open, deep water wave source areas. This choice of velocity is consistent with our assumption that the major portion of ice cover modification and an associated slow advance of wave energy takes place during the first of the two stages of our basic model. Consequently, the cited minimum significant waveheight requirement would have had to be satisfied, roughly, 220 km to the east of PA3 at, approximately 2000, March 20.

Independent estimates of sea states were made for a point 250 km due east of PA3 using 10 m winds calculated from the available Japan Meteorological Agency Analysis charts. This effort involved conversions of geostrophic estimates into equivalent 10 m winds, incorporating boundary layer reductions through use of multiplicative scaling factors and counter-clockwise rotations (Overland, 1985). Use of mid-range values for both adjustments, corresponding to a 0.66 scaling factor and a 30° rotation, suggested that surface winds from the ESE to ENE sector were present for an approximately 23 hour period preceding 2000, March 20 (Table 4). These winds were used in conjunction with a Bretschneider wave model nomograph (Bretschneider, 1969) to derive a sea state for the latter time characterized by a significant wave period of 16 s and a significant wave height of 12.7 m, contingent on the availability of a minimum fetch of approximately 580 km. The latter condition was easily satisfied on the basis of the March 21 SSM/I data, justifying some confidence in an estimate well in excess of our minimum sea state requirement. This apparent overestimation of source area sea states relative to expectations on the basis of PA3 wave intensity data is hardly surprising given the strong dependence of our estimates of the attenuation rates and propagation speeds assumed for ice fields east of the monitoring areas. Uncertainties may also be expected in the hindcast sea states through the necessary reliance on analyzed pressure contour data for wind velocity estimation. In the latter respect, it is interesting to note that the peaking of PA3 wave intensity at a time subsequent to an inferred transition to stage 2 behaviour is consistent with a subsequent increase in wind speed, albeit at a less favourable directionality (Table 4).

Time Interval	Speed (m/s)	Direction (from)
21:00, March 19-00:00, March 20	16.0	ESE
03:00-09:00, March 20	24.1	ESE
09:00-15:00, March 20	34.3	E
15:00-21:00, March 20	30.0	ENE
21:00, March 20-03:00, March 21	40.2	NNE

Table 4. 10m wind speeds and directions as computed as described in the text from the Japan Meteorological Agency charts for a location 250 km east of PA-3.

4.4 Temporal Variations in Wave Intensity: Inshore/Offshore Site Differences

As noted in Section 3, time series plots of wave intensity within the array of six central monitoring sites show both significant east to west enhancements of longer period temporal wave intensity modulation and longer event durations at inshore sites. These features of the data are likely manifestations of spatial inhomogeneities in the diverging ice pack. Such inhomogeneities are often evident on the East Sakhalin Shelf as alternating east-west bands containing, respectively, compact concentrations of vast floes and mixtures of smaller ice fragments, thin ice and open water. Drifts of alternating bands of these two very different kinds of ice across incident wave paths would produce significant temporal variations in wave attenuation and, hence, in wave intensity. It is suggested that periodic intervals of low wave intensity at an inshore site may have been consequences of the directly seaward presence of bands of compact ice. In this simple picture, the period of intensity variation, τ , can be written in terms of a southward ice drift velocity, v_i , and an inhomogeneity wavenumber, $K=2\pi/\lambda$ (where λ is the spatial periodicity of the ice cover banding) as:

$$\tau = (v_i \cdot K)^{-1}. \quad (3)$$

Identifying τ with the approximately 3.3 hour separations of observed successive intensity minima (Figure 9) and equating v_i to a coincident 1 m/s ice drift velocity, Eq. (3) yields a value of 12 km for λ , corresponding well with the typical average north-south dimensions of individual, southward drifting ice bands observed in the study region.

It is possible to make rough estimates of the effective wave coefficients, α_L , associated with the postulated low transmissivity ice bands using the relative magnitudes of adjacent wave intensity minima (I_{\min}) and maxima (I_{\max}) in Figure 9. Such estimates employ Eq. 1 in conjunction with approximate values of corresponding high transmissivity band attenuation coefficients, α_H , and the east-west separation, ΔL , between the outer edges of these bands and the measurement site. The quantity α_L can then written as:

$$\alpha_L = \alpha_H + (\ln(I_{\max}/I_{\min}))/2\Delta L. \quad (4)$$

Estimates of α_L for the PA1 site can be obtained using values of α_H equal to the attenuation coefficients listed in Table 2 for PA3 and PA2 vertices since such values were computed using maximal local intensities in more seaward areas. The two vertex estimates were combined into a single effective high transmissivity band value $\alpha_H = 3.0 \times 10^{-5} \text{ m}^{-1}$. Estimation of ΔL is more problematic in the absence of good contemporary image data. We chose to identify the edge of the low transmissivity bands with the 65% ice concentration contour as deduced from the March 21 SSM/I ice condition mapping. This choice yielded a value of $\Delta L = 65 \text{ km}$ with an estimated +/- 25 km uncertainty. Substitution of these parameters and the approximate observed (Figure 9) ratio $I_{\max}/I_{\min} \approx 4$ into Eq. 4 yields a value of $\alpha_L = 5.1 \times 10^{-5} \text{ m}^{-1}$ which is very close to values estimated above (Table 2) for regions occupied by the heavier, more compact ice in the vicinity of the most shoreward central sites. Allowing for parameter estimation uncertainties, this

result suggests that the observed oscillations in inshore temporal wave intensity are equivalent to roughly 50% to 100% modulations of the effective attenuation coefficients by the southward-drift of ice bands with wave transmission characteristics comparable to those associated with the heavier shoreward ice.

4.5 The First (Break-up) Stage of the Waves-in-Ice Event

Circumstantial evidence has been presented above to support the proposition that, at times close to and after initial steep rises in local wave activity, the March, 1998 waves-in-ice event can be reasonably well understood in terms of the expected properties of a concentrated, diverging collection of ice floes. A more complete description of the reported observations still requires identification of the process(es) involved in the postulated first stage of the event, characterized by anomalously slow and shoreward-decreasing speeds of wave energy propagation.

The LMC interpretation of the 1986 Antarctic waves-in-ice event, outlined in Section 1, is an obvious candidate for describing this critical phase of the event. Key elements of this interpretation are the derived (Liu and Mollo-Christensen, 1988) expressions for the phase and group velocities:

$$v_p(k) = [(gk + Bk^5 - Qk^3)/(1 + kM)]^{0.5}/k \quad (5)$$

and

$$v_g(k) = [g + (5 + 4kM)Bk^4 - (3 + 2kM)Qk^2]/[2v_p(1 + kM)^2], \quad (6)$$

where k is the wavenumber ($2\pi/\lambda$), $B = Eh^3/12(1 - s^2)\rho_w$, $Q = Ph/\rho_w$, $M = \rho_i h/\rho_w$ and g , E , s and P denote, respectively, the acceleration of gravity, Young's modulus of elasticity, Poisson's ratio and the compressive ice pack stress. As noted in Section 1, a common stress value ($P = 5.1 \times 10^6 \text{ N m}^{-2}$) was identified for the Antarctic event which produced both a, roughly, two-fold reduction in v_p from its zero-stress value and a near-zero value of v_g . The latter result would have created high local concentrations of wave energy, producing the rapid, spatially-progressive break-up and stress relief in the ice cover and leading to the lower wave attenuation rates and "normal", larger, phase velocities associated with the second stage of the event.

Unfortunately, our measurement array did not provide spatial wavelength data, precluding possible observations of anomalously short wavelengths equivalent to those reported for the early portion of the Antarctic event. Consequently, our evaluations of an LMC-like mechanism underlying the Sea of Okhotsk event must be focused upon comparisons between the observed low speeds of wave energy propagation and theoretical expectations in terms of a stress-dependent group velocity (Eq. 6).

The availability of concurrent data on ocean currents, ice drift and the basic character of the ice (i.e. draft and concentration) at the monitoring sites provide a quantitative basis for judging the feasibility of attaining the critical LMC stress value:

$$P_{\text{crit}} = \rho_w [g + (5 + 4kM)Bk^4] / [h(3 + 2kM)k^2], \quad (7)$$

associated with zero group velocity. Retaining the $h = 2$ m effective ice thickness assumed by LMC to account for the presence of ice ridging and deformation and choosing a values of k appropriate to the shorter, 14s, observed wave period, attainment of zero group velocities in the Sea of Okhotsk event would have required the presence of internal ice stresses approaching 5×10^6 N/m². Given that the slow advance of wave energy through the central study region occurred between, approximately 2100, March 20 and 0300, March 21, these stresses would have had to be present in a period in which the affected pack ice was undergoing rapid southward ice drift driven by strong northerly winds and intense southerly currents. Such circumstances are not compatible with the presence of the large shoreward (westward) stresses on the ice pack required by the LMC mechanism. The one obvious source of shoreward forcing in this period, arising from Coriolis forces directed to the right of ice drift, was found to be two orders of magnitude weaker than required even when 100 km of 2 m thick ice was assumed to be drifting southward seaward of the PA3 site. The demanding nature of the LMC threshold is such that even if the largest magnitude winds estimated for offshore wave source areas during the event (Table 4) were directed westward over such an ice cover, the resulting internal ice stress at PA3 would have still fallen short of the critical value by almost an order of magnitude. Consequently, although the earlier occurrence of an LMC process-driven event, as suggested by Liu and Mollo-Christensen (1988), cannot be ruled out because of the much larger seaward extents of the contemporary Antarctic ice pack, it is extremely unlikely that a similar mechanism was involved in the event considered in the present study.

In the absence of additional data, a simple alternative explanation for the first, break-up, stage of a two stage mechanism can be constructed by abandoning LMC's direct association between anomalously low speeds of wave energy propagation and altered wave group velocities. Instead, given the heavily compacted and deformed nature of the ice cover immediately prior to the March 20 wind rotation and its accompanying changes in forcing, subsequent waves incident on the ice cover would have been expected to be, initially, rapidly damped out, creating a zone of broken ice along the outer boundary of a, still, highly wave-attenuative ice cover. Over time and with continued exposure to large incident waves, this zone of broken ice should have expanded westward along the wave propagation direction. Such an expansion and accompanying reductions in local wave attenuation rates in areas progressively further inside the pack would have been facilitated by the above-noted divergences in the ice and upper ocean flows. It is also conceivable that the rapidity of the inferred transition to "normal" wave transmissivity could have been a consequence of the combined sustained intensity of the pre-1800, March 21 ice deformations and the subsequent sudden switch from westward to southward forcing. This sequence may have created an initially very compact, but largely unconsolidated, mass of highly broken ice with extremely low resistance to immediately

subsequent divergence. If valid, such an interpretation would suggest that the recent dynamical history of an ice cover is not inconsequential in the development of realistic models of its subsequent behaviour.

Some evidence for this interpretation and the critical importance of divergent flow may lie in the absence of wave activity at the northernmost, Levenshterna, site. As noted earlier, this absence was anomalous in view of the site's greater proximity to open water and, given the dimensions and track of the traversing cyclone (Figure 1), the apparent exposure of this site to open ocean sea states comparable to those attained east of the central sites. Consequently, a primary distinction of the Levenshterna site was the absence of sequential exposure to easterly and then northerly winds of strength sufficient to, first, produce deformations comparable to levels attained at the central sites and, then, to drive equivalently large southward ice drift- and current- components (Figures 6 and 9). A drastic shortfall in this respect was evident in the extent of the westward forcing: suggesting that initial local compression could have been a major determinant of local ice cover responses to the wind and current changes which initiated intense waves-in-ice activity in more southern areas.

5. Summary and Conclusions

This study has confirmed the existence of previously reported (Liu and Mollo-Christensen, 1988) large amplitude wave activity well inside the boundaries of a large body of thick pack ice. Data from a large array of moored, sub-surface ice draft, ice velocity and current sensors provided quantitative information on spectra, attenuation rates, directions and speeds associated with propagation of wave energy into the ice pack. This information offers a substantial, if still not complete, basis for understanding relationships between intense waves-in-ice events and environmental forcing factors.

Although a full comparison of the obtained results with the observations reported by Liu and Mollo-Christensen (1988) was limited by the absence of spatial wavelength data, it was established that anomalously large waves-in-ice amplitudes can be observed in the absence of the extremely large contemporary compressive internal ice stresses postulated by the latter authors. As in the earlier work, the observed event was interpretable in terms of two stages, the second of which consisted of relatively "normal" propagation of waves through concentrated collections of ice floes. Wave attenuation in this stage of the event is attributable, primarily, to multiple wave scattering at floe boundaries.

Less clarity was achieved in identifying mechanisms underlying the event's first stage associated with anomalously slow wave energy propagation. Thus, although static stress-induced reductions in wave group velocities invoked by Liu and Mollo-Christensen (1988) to explain the Antarctic waves-in-ice event were insignificant factors in this instance, a detailed alternative explanation for our observations remains to be established. The data suggest that such an explanation is likely to be dependent on the presence of divergence in the ice drift field. Such divergence was initiated by a wind rotation which, rather suddenly, introduced strong southward movement into a previously westward- (shoreward-) driven deforming ice pack. Indirect evidence from spatial differences in ice

responses to nominally similar incident source area wave fields suggests that the intensity of an initial compressive deformation and the rapidity of a subsequent switch to divergent forcing may have been critical to effecting a transition to higher wave transmissivity in the postulated second stage of the waves-in-ice event.

Clearly, additional efforts are required to better establish details and ranges of possibilities for large waves-in-ice occurrences. Pairings of moored ice and current profilers are potent tools in such efforts, offering demonstrated capabilities for safe, robust recovery of data from severe, exposed, pack ice environments. An important addition to future similar wave study-directed programs should be a capability for direct measurement of spatial wavelengths. Although some assistance in this regard could be expected from all weather radar imagery, this capability should be achievable through inclusion of a small number (3) of closely spaced (i.e. shorter than the smallest anticipated wavelength) ice profilers at each or selected sites in larger regional monitoring arrays.

6. Acknowledgements

The author wishes to acknowledge the essential access to JIP data provided by Exxon and Sakhalin Energy as well as the encouragement and helpful comments offered by their personnel, Dr. John Heideman and Mr. Kenneth Schaudt. Other key contributions were regional meteorological analysis data provided by the Japan Meteorological Agency and numerous suggestions and reviews by Drs. R.T. Thomson and H. Melling of the Institute of Ocean Sciences, Sidney, B.C. and by David Fissel of ASL Environmental Sciences Inc. Other ASL staff members such as Rick Birch, Keith Borg, Ryan Greeley and Ed Ross also made essential contributions in terms of instrument deployment and recovery, data processing and graphics preparation.

References

- Birch, J.R., D. Fissel, H. Melling, K. Vaudrey, K. Schaudt, J. Heideman and W. Lamb. 2000. Ice Profiling Sonar: Upward looking sonar provides over-winter records of ice thickness and ice keel depths off Sakhalin Island, Russia. *Sea Technology*, August Issue, pp. 48-53.
- Bretschneider, C.L., 1969. Wave Forecasting. In *Handbook of Ocean and Underwater Engineering*, edited by J.J. Myers, C.H. Holm and R.F. McAllister, McGraw-Hill, New York, pp.11-97-11-109.
- De Leonibus, P.S., 1963. Power spectra of surface wave heights estimated from recordings made from a submerged hovering submarine. In *Ocean Wave Spectra*, Prentice-hall, Englewood cliffs, N.J., pp.243-249.
- Fox, C. and V.A. Squire, 1990. Reflection and transmission characteristics at the edge of shore fast sea ice. *J. Geophys. Res.*, **95**, pp. 11629-11639.
- Liu, A. K. and E. Mollo-Christensen, 1988, Wave propagation in a solid ice pack. *J Phys. Oceanogr.*, **18**, pp.1702-1712.
- Marko, J.R., 1998. Evaluation and development of Radarsat imagery for use in support of oil production in the Sea of Okhotsk. Report prepared for Canada Centre for Remote Sensing, Canada Space Agency, Ottawa. 24p. plus figures.

Macovsky, M.L. and G. Mechlin, 1963. A proposed technique for obtaining directional wave spectra by an array of inverted fathometers. In *Ocean Wave Spectra*, Prentice-Hall, Englewood Cliffs, N.J., pp.235-241.

Meylan, M.H., V.A. Squire and C. Fox, 1997. Toward realism in modeling ocean wave behavior in marginal ice zones. *J. Geophys. Res.* **102**, pp. 9029-9049.

Overland, J.E., 1985. Atmospheric boundary layer structure and drag coefficients over sea ice. *J. Geophys. Res.* **90**, pp. 22981- 22992.

Rufenach, C.L. and A.K. Liu, 1995. Comment on “Geophysical and oceanographic information in the marginal ice zone from ocean wave measurements” by Vernon Squire. *J. Geophys. Res.*, **100**, pp.8849-2972.

Rothrock, D.A., and A.S. Thorndike, Measuring the sea ice floe size distribution. *J. Geophys. Res.*, **89** (C4), 6477-6486, 1984.

Squire, V.A., 1995, Geophysical and oceanographic information in the marginal ice zone from ocean wave measurements, *J. Geophys. Res.*, **100**, pp.997-998.

Squire, V.A. and S.C. Moore, 1980. Direct measurement of the attenuation of ocean waves by pack ice. *Nature* **283**, pp. 365-368.

Wadhams, P., 1978. Wave decay in the marginal ice zone measured from a submarine. *Deep-Sea Research* **25**, pp 23-40.

Wadhams, P. 1986. The seasonal ice zone. in *The Geophysics of Sea Ice* (N. Untersteiner, ed.), Plenum Press, New York and London, pp. 825-991.

Wadhams, P., V.A. Squire, D.J. Goodman, A.M. Cowan and S.C. Moore, 1988. The attenuation rates of ocean waves in the marginal ice zone. *J. Geophys. Res.* **93**, pp. 6799-6818.